Chapter 3

Regional-scale model

3.1 Theory

3.1.1 ICBL budget method

In fair weather conditions the daytime atmospheric boundary layer is generally well mixed by turbulence generated by thermal convection. The height of the convective boundary layer (CBL) grows during the day as thermal plumes overshoot the capping inversion and entrain overlying air into the CBL. A mass balance shows that the rate of change of scalar storage in the CBL is a function of the growth rate of the CBL, the vertical velocity at the top of the CBL, the scalar concentration of air being entrained and the surface scalar flux (eg. Lloyd *et al.*, 2001):

$$\frac{d\left(M_B c_B\right)}{dt} = c_+ \frac{dM_B}{dt} + \left(c_B - c_+\right) W_+ + F_c \tag{3.1}$$

where the subscripts B and $+$ refer to the mean values within and just above the boundary layer, respectively; $M_B = \rho_B h$ is the number of moles of air per unit ground area in the CBL, with ρ being the molar air density and h the height of the CBL; c is the scalar concentration; F_c is the surface flux of scalar c; and $W_+ = \rho_+ w_+$ is the mass flux per unit area into or out of the boundary layer due to the mean vertical velocity w_+, defined as positive upwards. Here it is necessary that h be defined as the height just above the entrainment zone, so that a positive w_+ results in a loss of air at concentration c_+ through

the top of the boundary layer, and a compensating gain of air at concentration c_B through the sides of the column of air under consideration. The reverse is true for a negative w_+ (subsidence). The gradient in scalar concentration above the CBL is assumed to be zero, a reasonable assumption for CO_2 and its isotopes according to the data obtained in this study. An equivalent equation is derived in Raupach (2000, his Equation (A9)) as a special case of the conservation equation in a moving region with spatially variable fluid density.

Assuming the scalar concentration above the boundary layer is constant in time, Equation (3.1) can be integrated to relate mean conditions at two different times during the day to the average surface flux over that period to obtain the integral CBL (ICBL) budget equation (Lloyd *et al.*, 2001):

$$\langle F_c \rangle = \frac{(c_{B1} - c_+) M_{B1} - (c_{B0} - c_+) M_{B0}}{T} - (\langle c_B \rangle - c_+) \langle W_+ \rangle \tag{3.2}$$

where angle brackets denote time averaging and T is the integration period from time t_0 to t_1. The average of the product of quantities in the subsidence term is approximated by the product of their averages. In practice, the averages are estimated from the mean of values at consecutive sampling times.

Relaxing the assumption of constant free tropospheric concentration gives an additional contributing term:

$$\langle F_c \rangle = \frac{(c_{B1} - c_{+1}) M_{B1} - (c_{B0} - c_{+0}) M_{B0}}{T} - (\langle c_B \rangle - \langle c_+ \rangle) \langle W_+ \rangle + \frac{1}{T} \int_{t_0}^{t_1} M_B \frac{dc_+}{dt} dt \tag{3.3}$$

To evaluate the additional term (the last term in Equation (3.3)) we can approximate the integral by treating the terms within as independent and integrating each separately as was done for the subsidence term in Equation (3.2). This then leads to an equation identical to Equation (3.2) except that average free troposphere concentrations are used:

$$\langle F_c \rangle = \frac{(c_{B1} - \langle c_+ \rangle) M_{B1} - (c_{B0} - \langle c_+ \rangle) M_{B0}}{T} - (\langle c_B \rangle - \langle c_+ \rangle) \langle W_+ \rangle \tag{3.4}$$

where again the time average is calculated as the mean of values at consecutive sampling times, $\langle c_+ \rangle = (c_{+1} + c_{+0})/2$. If free tropospheric concentrations are assumed to be constant with height, then their variation with time implies that significant advection must be occurring. In this case one might expect that concentrations within the boundary layer may similarly be affected. Air flow above the boundary layer, however, is decoupled from that below, and advection above does not necessarily imply advection within. In addition, since scalar concentrations in the free troposphere are also decoupled from surface influences and the air there is stable, horizontal heterogeneity above the boundary layer may be preserved for several days in the absence of large-scale synoptic events. In contrast, mixing within the boundary layer occurs over several minutes.

3.1.2 Height integration method

The second approach investigated here calculates total mass or moles of scalar per unit ground area up to an arbitrary height where conditions are assumed to be constant with time, here taken to 3000 metres. This method was first applied by Wofsy *et al.* (1988) to infer regional CO_2 fluxes over the Amazon basin. The method doesn't require knowledge of h, but it requires the integrating region to extend high enough that vertical air flow is negligible or can be estimated and concentrations are invariant in both space and time. Differences in scalar molar density at different times can be equated to average surface flux over that period, so that:

$$\langle F_c \rangle = \frac{1}{T} \sum_i \left[(\rho_i c_i)_1 - (\rho_i c_i)_0 \right] \Delta z_i \tag{3.5}$$

where $T = t_1 - t_0$ is the integration period; i represents the layer from z_{i-1} to z_i; and $\Delta z_i = z_i - z_{i-1}$. Note that Equation (3.5) can be applied with only two layers being chosen:

within and above the CBL. With the assumption of time-invariant c_+ and no change in total moles of air in the integrating column, it then reduces to Equation (3.2) without the subsidence term, noting that the rate of change of moles of air per unit ground area in the CBL is equal to minus the rate of change of moles of air in the free troposphere, so that $M_{B1} - M_{B0} = -(M_{T1} - M_{T0})$, where $M_T = \bar{\rho}_T (3000 - h)$ is the moles of air per unit ground area in the free troposphere from h to 3000m.

A change in the average density within the integrating column from one time to the next implies that air has been gained or lost through the top or sides of the column. The density profiles obtained in this study showed that as the temperature increased during the day the air density near the ground decreased, while that above the CBL tended to increase slightly. The average density throughout the column decreased during the day. Assuming that air was lost through the top of the column, this loss can be accounted for by including an additional term involving the difference in average density:

$$\langle F_c \rangle = \frac{1}{T} \left\{ \sum_i \left[(\rho_i c_i)_1 - (\rho_i c_i)_0 \right] \Delta z_i - (\bar{\rho}_1 - \bar{\rho}_0) z_R c_R \right\} \tag{3.6}$$

where z_R is the height to which the integration is taken and c_R is the scalar concentration at that height (assumed to be time-invariant). A term can also be included to account for air flow through the top of the column that is compensated by horizontal flow (ie. subsidence) as in Equation (3.4) to obtain:

$$\langle F_c \rangle = \frac{1}{T} \left\{ \sum_i \left[(\rho_i c_i)_1 - (\rho_i c_i)_0 \right] \Delta z_i - (\bar{\rho}_1 - \bar{\rho}_0) z_R c_R \right\} + \langle W_+ \rangle \left(\langle c_+ \rangle - \langle c_B \rangle \right) \tag{3.7}$$

where the subsidence correction requires average concentrations within and above the CBL to be determined as in the integral budget method of Equation (3.4).

3.1.3 Application to isotopes of CO_2

Equations (3.4) and (3.7) can be applied to any scalar, including an isotope of a particular

species. Isotopic discrimination can then be calculated from application of these equations to both the scalar and its "iso-concentration" (isotopic composition times concentration, δc). Models of isotope discrimination during photosynthesis were presented in Chapter 2 but are reproduced here so that this chapter may be read and understood in isolation.

Isotopic composition is defined as $\delta = \frac{\mathcal{R}}{\mathcal{R}_{std}} - 1$, where $\mathcal{R} = \frac{c*}{c}$ is the ratio of concentration of minor to major isotope of scalar c, with the star indicating the minor isotope, and $\mathcal{R}_{std}$ is that for an isotopic standard of the same species. The flux of minor isotope is then given by $F_{c*} = \mathcal{R}_{std}\,(F_{\delta c} + F_c)$, where the product δc is treated the same as any other scalar, and the isotopic composition of the scalar flux is given by: $\delta_{F_c} = \frac{F_{c*}/F_c}{\mathcal{R}_{std}} - 1$. In the case of carbon dioxide, $\delta_{F_{CO_2}} = \frac{A\delta_A + R\delta_R}{A+R}$, where A is the net assimilation flux of CO_2 which includes leaf respiration, R is the combined root, soil and stem respiration flux, and δ_A and δ_R are the isotopic compositions of these fluxes. The sign convention adopted here is positive upwards, so that A is negative during the day as plants assimilate CO_2. Isotopic discrimination during assimilation is defined as $\Delta_A = \frac{\mathcal{R}_B}{\mathcal{R}_A} - 1 \approx \delta_B - \delta_A$, where the subscripts B and A refer again to ambient (within CBL) air and air carried by the assimilation flux, respectively. Discrimination is then given by:

$$\Delta_A = \delta_B - \frac{F_{\delta c} - R\delta_R}{F_c - R} \tag{3.8}$$

3.1.4 Modelling isotope discrimination during CO_2 assimilation

Physiological models of carbon and oxygen isotope discrimination were used to interpret the estimates obtained by the CBL budget methods (see also Chapter 2 for further detail and references). As in Chapter 2, carbon and oxygen isotopic composition of CO_2 is expressed on the PDB-CO_2 scale (relative to CO_2 derived from the Pee-Dee Belemnite calcite formation) and oxygen isotope composition of water on the SMOW scale (relative to Standard Mean Ocean Water). These scales are now strictly called VPDB-CO_2 and VSMOW, respectively, to reflect standardisation protocol penned at the International Atomic Energy Agency in Vienna, 1995, but the V prefix will be omitted here.

Carbon isotope discrimination

The simplest model for carbon isotope discrimination during plant uptake of CO_2 is given by $\Delta^{13}C = a + (b-a)c_i/c_a$ (Farquhar *et al.*, 1982), where a is the fractionation occurring due to diffusion in air (calculated as 4.4‰), b is the effective net fractionation during carboxylation (effective value measured as ∼27‰), and c_i and c_a are the intercellular and ambient partial pressures of CO_2, respectively. Estimates of carbon isotope discrimination and its diurnal or day to day variation therefore describe variation in intercellular CO_2 concentration with respect to ambient concentration.

Oxygen isotope discrimination

CO_2 entering the chloroplast equilibrates with water there, and exchange of oxygen atoms is catalysed by the enzyme carbonic anhydrase. Some of the CO_2 is assimilated but some diffuses back out of the leaf, carrying the isotopic signature of chloroplast water. Chloroplast water is enriched in heavy isotopes compared to source water because lighter isotopes are preferentially evaporated (Farquhar *et al.*, 1989b).

Isotopic composition of water at the sites of evaporation within the leaf, δ_e, is modelled by $\delta_e = \delta_S + \varepsilon_k + \varepsilon^* + (\delta_V - \delta_S - \varepsilon_k)e_a/e_i$, where δ_S is the oxygen isotopic composition of source water; δ_V is that of water vapour in the surrounding air; ε_k is the kinetic fractionation factor (28.5‰ through the stomata and 18.9‰ in the boundary layer and the effective fractionation is here taken as 26‰); ε^* is the proportional depression of equilibrium vapour pressure by the heavier molecule (9.4‰ at 25°C); and e_a and e_i are the vapour pressures in the ambient air and intercellular spaces, respectively. This equation was developed by Craig and Gordon (1965) for a free water surface and modified by Farquhar *et al.* (1989b) for application to the leaf, and is referred to as the Craig-Gordon model.

In analogy with the carbon case, oxygen isotope discrimination is modelled by $\Delta^{18}O = a_k + (\delta_c - \delta_a)c_c/(c_a - c_c)$ (Farquhar and Lloyd, 1993), where a_k is the weighted mean fractionation during diffusion to the sites of carboxylation (taken as 7.4‰); c_c and c_a are

the CO_2 concentrations in the chloroplast and ambient air, respectively; and δ_c and δ_a are the oxygen isotope composition of CO_2 in the chloroplast and ambient air, respectively. CO_2 is assumed to be in equilibrium with chloroplast water before fixation, and the isotopic composition of the latter is approximated by δ_e. Fractionation during equilibration is 41.2‰ at 25°C (O'Neill *et al.*, 1975: this is close to the difference between the PDB-CO_2 and SMOW scales of 41.47‰).

3.1.5 ICBL budgets of H_2O and sensible heat

Equation (3.4) can be applied without modification to water vapour, if it can be assumed that the gradient in H_2O concentration with height above the boundary layer is negligible. In the case of sensible heat, however, the stable air above the boundary layer means that there always exist significant gradients in virtual potential temperature there. Virtual temperature (T_v) is the temperature that dry air would have at the same density and pressure as moist air: $T_v = T(1 + 0.61q)$, where T is measured temperature and q is the specific humidity. Virtual potential temperature (here denoted by θ) is the virtual temperature that a parcel of air would have if brought adiabatically to a reference pressure, here taken as 100 kPa: $\theta = T_v(p/p_R)^{-R_m/c_p}$, where p and p_R are the measured and reference atmospheric pressures, respectively, and R_m is the gas constant for dry air.

Integration of Equation (3.1) to find the regional surface heat flux F_H then proceeds by noting that $\frac{d\theta_+}{dt} = \gamma_\theta \frac{dh}{dt}$, where θ_+ is the virtual potential temperature just above the boundary layer and γ_θ is the gradient in θ_+ with height. Equation (3.1) then becomes:

$$\frac{d\left(M_B \Delta_\theta\right)}{dt} = -\gamma_\theta M_B \frac{dh}{dt} + \Delta_\theta W_+ + \frac{F_H}{c_p}$$

where $\Delta_\theta = \theta_B - \theta_+$, the difference in virtual potential temperature across the top of the boundary layer. Integration of this equation leads to the following relation for calculation of regional sensible heat flux:

$$\langle F_H \rangle = c_p \left\{ \frac{\left(\Delta_{\theta 1} M_{B1} - \Delta_{\theta 0} M_{B0}\right) + \frac{\gamma_\theta}{2}\left(M_{B1} h_1 - M_{B0} h_0\right)}{T} - \langle \Delta_\theta \rangle \langle W_+ \rangle \right\} \qquad (3.9)$$

where time variation in average boundary layer density has been assumed to be insignificant compared to variation in boundary layer height, and it is assumed that the vertical gradient in virtual potential temperature above the boundary layer is constant.

3.2 Methods

Profiles of CO_2 concentration, temperature, humidity and pressure were obtained in and above the convective boundary layer at a remote field site in central Siberia near the town of Zotino, at 61°N, 89°E. Flask samples of air were taken for isotopic analysis of CO_2. Two flights were made in mid-summer on 23 July 1998 at 14:00 and 21:00, and three on 24 July 1998 at 08:00, 14:00 and 19:00 (all times are local standard times, UTC+7).

Surface fluxes were measured from towers on the ground by the eddy covariance technique at two sites reflecting the two dominant ecosystem types in the area: forest and bog. NDVI data for the region suggest that the ratio of forest to bog area is about 5 (Lloyd *et al.*, 2001). The ground-based measurements at the bog site are described in detail in Arneth *et al.* (2002b) and Kurbatova *et al.* (2002), and those at the forest site are described in Tchebakova *et al.* (2002), Lloyd *et al.* (2002b) and Shibistova *et al.* (2002). These measurements cannot be considered to be representative of the entire region sampled by the CBL budget methods, but give an indication of the magnitude of fluxes to be expected from the two major ecosystem types in the region.

Atmospheric sampling protocol and corrections to raw data were the same as reported in Lloyd *et al.* (2002a), with the main points being described here. CO_2 concentration within the atmospheric boundary layer was measured with a LICOR 6251 infra red gas analyser (IRGA) operated in absolute mode, temperature and humidity were measured with a Vaisala HMP35D capacitive humidity sensor and PT100 platinum resistance sensor, and pressure with a Vaisala PTB101B aneroid barometer. Output was logged at 1 Hz frequency on a Delta T DL3000 datalogger. An Antonov AN2 plane was used with air intake and temperature/humidity sensor attached to the port wing. The engine exhaust

was located on the starboard wing. Flask samples of air were obtained with a system based on that used by the Global Atmospheric Sampling Laboratory (GASLAB), CSIRO Atmospheric Research, Australia. One-litre flasks had been preconditioned by heating and flushing with nitrogen. During sampling flasks were flushed for four minutes with dry air (passed through a magnesium perchlorate trap) at ambient pressure then pressurised to two bars absolute pressure and analysed at GASLAB for concentrations of CO_2 and carbon and oxygen isotopic composition of CO_2.

During each flight profiles were obtained over both a forest-dominated area (*Pinus sylvestris* with moss and lichen ground cover) and a bog-dominated area (*Sphagnum* and *Carex* species, *Scheuchzeria palustris* and *Andromeda polifolia*). Sampling of CO_2 concentration, temperature and pressure would begin 50-100 metres above the ground and run continuously with flask sampling at intervals while ascending to 3000 metres in a spiral of $\sim$2 km radius. A similar descending spiral would then be made over the second sampling area. Typically six to eight flasks were filled during each profile, generally at heights around 50-100m, 200m, 500m, 1000m, 1500m, 2000m, 2500m and 3000m for both the ascent and descent. Zero and span on the IRGA were adjusted at the start of each flight using nitrogen and two reference CO_2 gases at 340 and 380 ppm, respectively. Reference gas was also run through the IRGA during each flask-sampling period for later correction of any drift. The correction was applied by interpolating the offset of reference values and subtracting this offset from the sample concentrations. This calibration also accounted for any pressure correction required in addition to the standard correction applied according to the LICOR software. Each ascent and descent typically took about half an hour each to complete. Comparison of the two profiles obtained during each flight showed no discernible change in concentrations during the flight, indicating that the profiles could be treated as approximately instantaneous. Since the ascent and descent profiles corresponding to forest and bog areas were generally indistinguishable (see §3.4), the profile pairs were averaged and the times nominated for averaged profiles were roughly the median times for each pair.

Virtual potential temperature was calculated from measured temperature, pressure and humidity. Height was calculated from pressure data using the hydrostatic equation to obtain (see Appendix E for derivation):

$$z = \frac{T_0}{\gamma}\left[1 - \left(\frac{p}{p_0}\right)^{\frac{R_m\gamma}{g}}\right] \tag{3.10}$$

where p is the pressure at height z; p_0 is that at the ground; T_0 is the virtual temperature at the ground; γ is the adiabatic lapse rate; R_m is the gas constant for dry air; and g is the acceleration due to gravity.

Temperature data were corrected for sensor lag according to the equation (see Appendix F for derivation):

$$T_{real} = T_{meas} + \frac{\beta}{k} \tag{3.11}$$

where T_{real} is the true temperature; T_{meas} is measured temperature; β is the time rate of change of temperature during the flight, assumed to be constant (see Appendix F for justification); and k is the inverse time constant of the sensor.

Equation (3.11) shows that the effect of sensor lag is to offset the measured temperature from the real temperature by a constant amount relating to the rate of change in ambient temperature (which depends on the rate of ascent) and the time constant of the sensor. The factor β was calculated as the slope in temperature with time for the two minutes surrounding each measurement, and the factor $\frac{1}{k}$ was estimated as 80 seconds. These values gave very good agreement in temperature for the ascending and descending profiles. With no correction the two temperature profiles were offset by about 3°C. Though the same sensor was used for humidity measurements, the lag correction was required only for temperature because of the thermal mass of the instrument. Relative humidity measurements made by the instrument were converted to absolute humidity and molar vapour concentration using the measured rather than the ambient temperature.

To reduce scatter due to horizontal inhomogeneity, average [CO_2], [H2O], virtual potential temperature and air density were calculated for each 50-metre interval up to 3000m. The height of the boundary layer was estimated from the CO_2 and water vapour concentration jumps and level of the temperature inversion. The source codes for calibrations, corrections and averaging are given in Appendix H.

3.3 Results

3.3.1 Meteorological conditions

Model data provided by the National Centers for Environment Prediction (NCEP) Reanalysis Project for the 60°N, 90°E gridpoint (within ∼70 km of the study site) suggest mean vertical velocities above the CBL of -0.001 ms^{-1} on the afternoon of 23 July and night of 23-24 July, -0.004 ms^{-1} in the morning of 24 July and -0.005 ms^{-1} on the afternoon of 24 July. The sign convention is positive upwards, so these velocities imply subsidence of the CBL. Mean vertical velocity at the top of the CBL could also be estimated from the drop in height overnight of the top of the CBL, as seen by the height of the residual layer. The velocity thus found, -0.008 ms^{-1}, was considerably larger than the NCEP model estimates. Since the value of -0.008 ms^{-1} was found from observed data and the comparison of the NCEP model estimates for the corresponding period was not good, this value was used for the entire study period, from mid-afternoon on 23 July to the evening of 24 July (the validity of this extrapolation is discussed in §3.4). The contribution of the subsidence term to the inferred assimilation flux for each integration period was around -1.8 μmol $m^{-2}s^{-1}$.

Mean sea level pressure obtained from NCEP showed that a large high pressure region was present to the north of the study site and this was fairly stable during the study period (Figure 3.1). Individual flight trajectories carried out as described in Lloyd *et al.* (2002a) showed that the prevailing winds for all flights in this study originated from a northerly direction.

3.3.2 Observations of scalar concentrations and isotopic composition within and above the atmospheric boundary layer

Profiles of CO_2 and its carbon and oxygen isotopic composition on the afternoon and evening of 23 July show vertical structure typical of a well-mixed atmospheric boundary layer, with concentrations fairly constant within and a sharp jump at its top (Figures 3.2a, 3.3a and 3.4a). Average CBL CO_2 concentration in the afternoon was less than that in the evening because although net surface uptake was occurring, the boundary layer grew considerably in the intervening period, entraining free tropospheric air of much higher concentration (Figure 3.2a). This pattern was also present in the profiles where the surface discrimination was positive but the carbon isotope composition of CO_2 in the CBL decreased in the evening due to entrainment of CO_2 of lighter carbon isotope composition (Figure 3.3a). The oxygen isotope composition, however, increased significantly in the evening of 23 July due to the combined effects of entrainment of heavier (in oxygen isotopes) CO_2 and positive surface discrimination during that period (Figure 3.4a).

The morning profiles on 24 July show very high CO_2 concentrations and low carbon and oxygen isotope composition in the nocturnal boundary layer (NBL) up to about 100m (Figures 3.2b, 3.3b and 3.4b). The residual layer concentrations in the morning and CBL concentrations in the afternoon and evening are very similar, and very little variation in boundary layer depth is observed (Figure 3.2b). This is also evident in the carbon and oxygen isotope profiles (Figures 3.3b and 3.4b). The profiles on this day do not allow immediate inferences to be drawn about the sign of the surface exchange, except for the obvious influence of respiration overnight with its lighter isotopic composition.

Profiles of virtual potential temperature clearly show the temperature inversion at the top of the boundary layer for each flight (Figure 3.5). The morning profile on 24 July also shows a strong inversion within the NBL. The vertical gradient in virtual potential temperature above the boundary layer was estimated from the measured profiles as 0.003 Km^{-1}, constant over the two-day period. Profiles of water vapour within and above the CBL show a strong anti-correlation with CO_2 (Figure 3.6), demonstrating the correlation

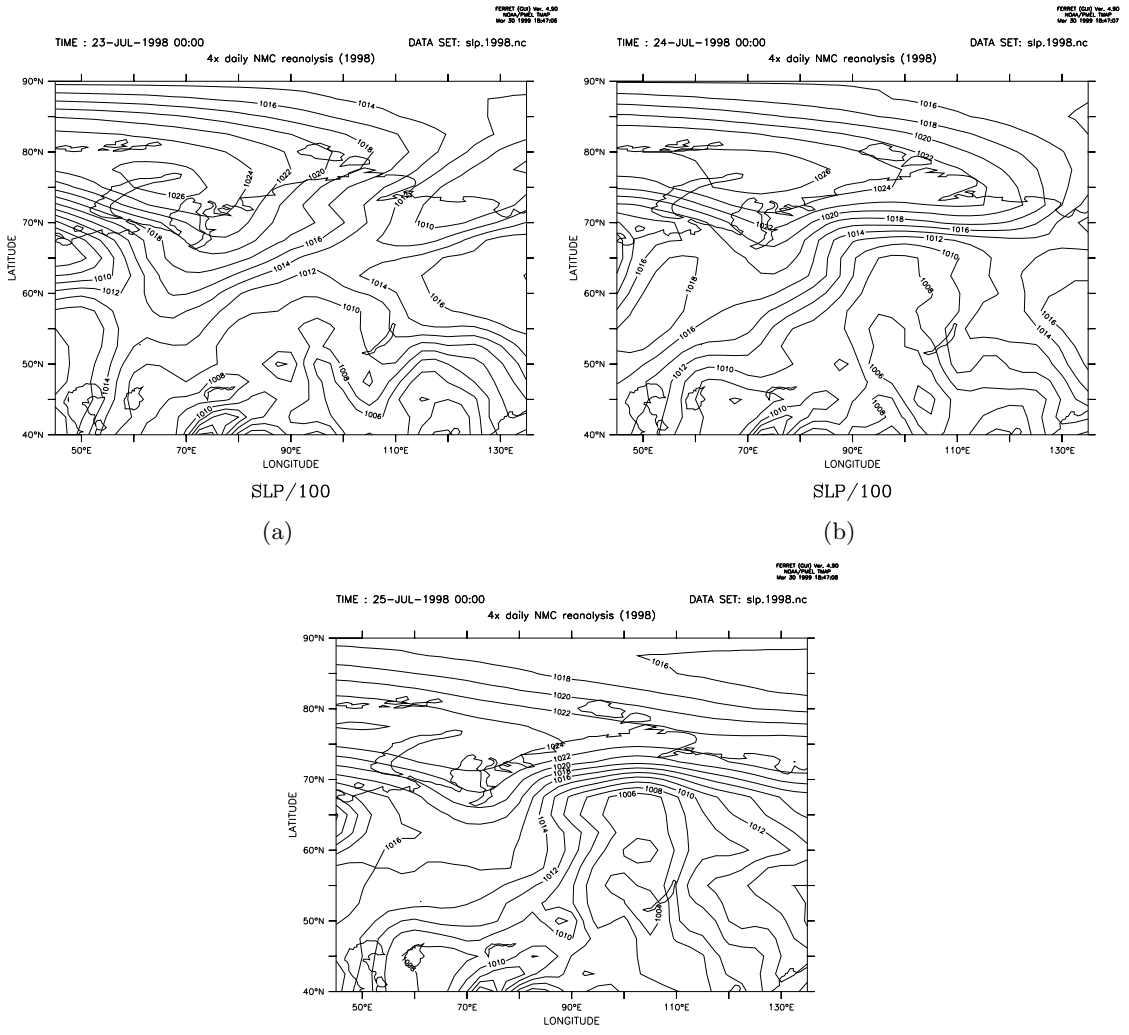

Figure 3.1: Mean sea level air pressure surrounding the study region during the experiment, at 00:00 UTC (0700 h local time) on (a) 23 July 1998; (b) 24 July 1998; and (c) 25 July. The study region was located at around 60.6°N, 89.5°E.

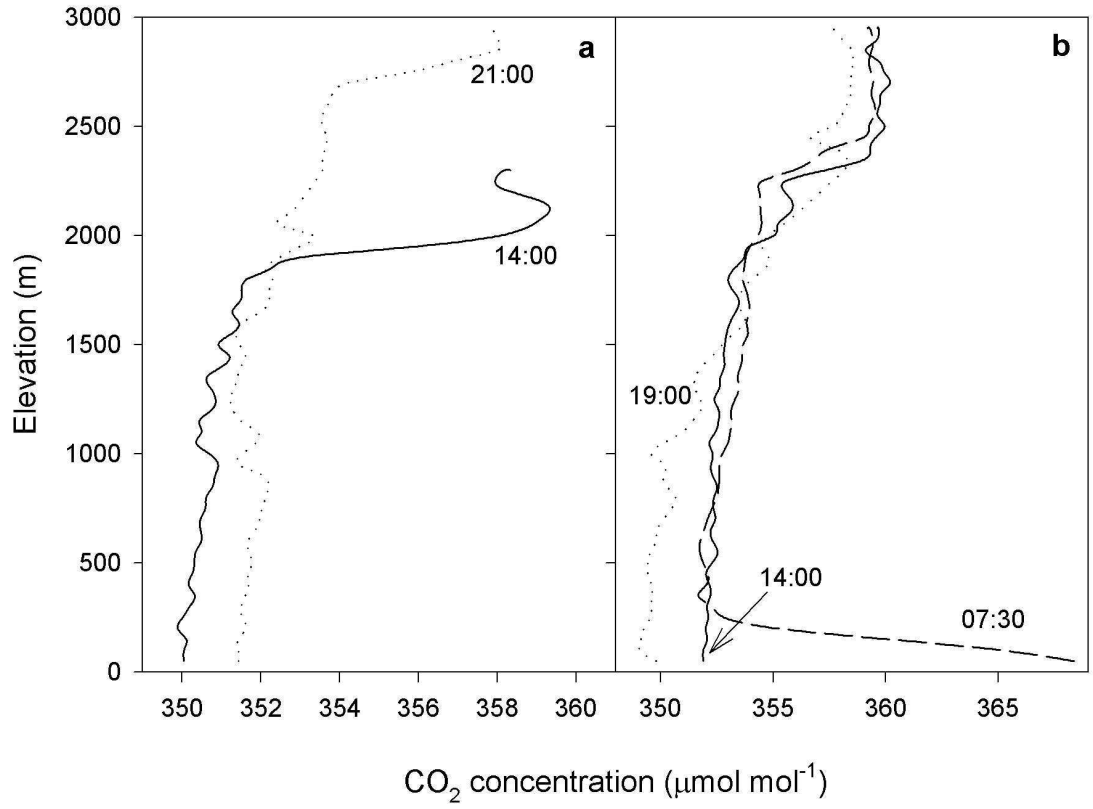

Figure 3.2: Profiles of CO_2 concentration on (a) 23 July 1998 and (b) 24 July 1998. Concentration was monitored continuously and averaged over each 50-metre interval. Solid line is the afternoon profile (14:00 on each day), dotted line is the evening profile (21:00 on 23 July, 19:00 on 24 July) and dashed line is the morning profile (07:30 on 24 July).

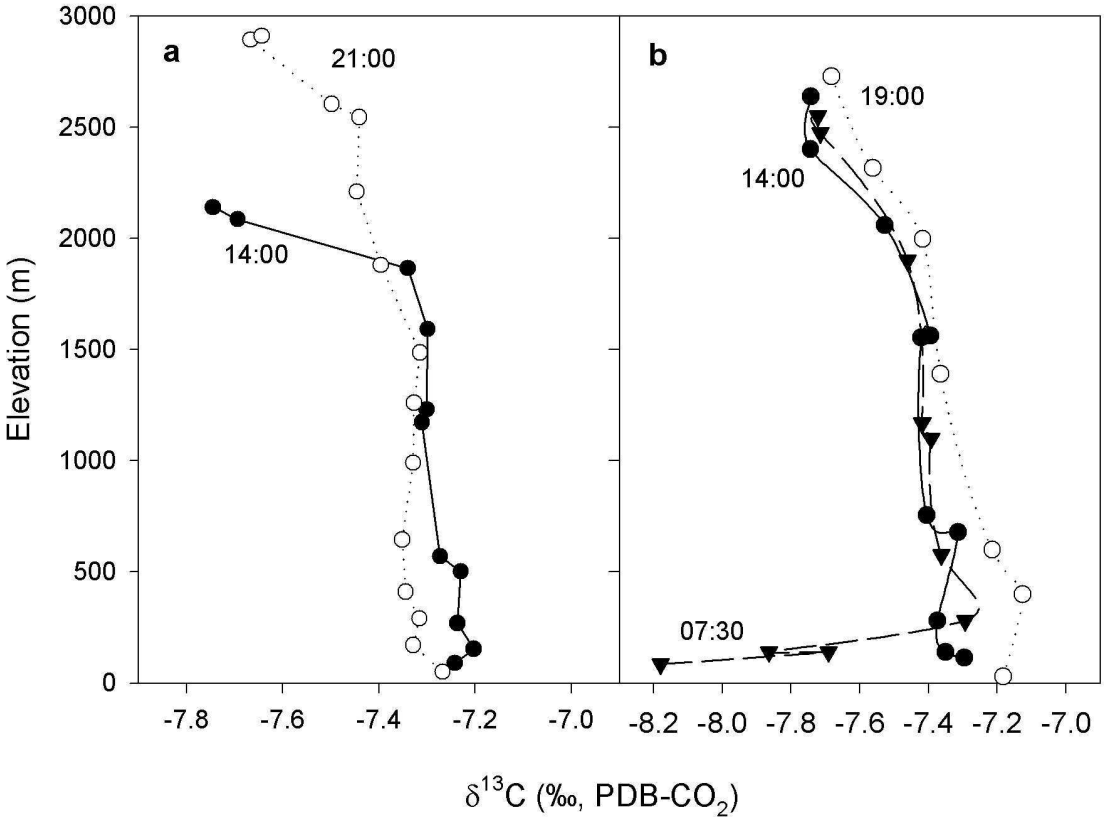

Figure 3.3: Profiles of δ^{13}C composition of CO_2 on (a) 23 July 1998 and (b) 24 July 1998. Symbols indicate where flask samples were taken. Solid line with filled circles is the afternoon profile (14:00 on each day), dotted line with open circles is the evening profile (21:00 on 23 July, 19:00 on 24 July) and dashed line with filled triangles is the morning profile (07:30 on 24 July).

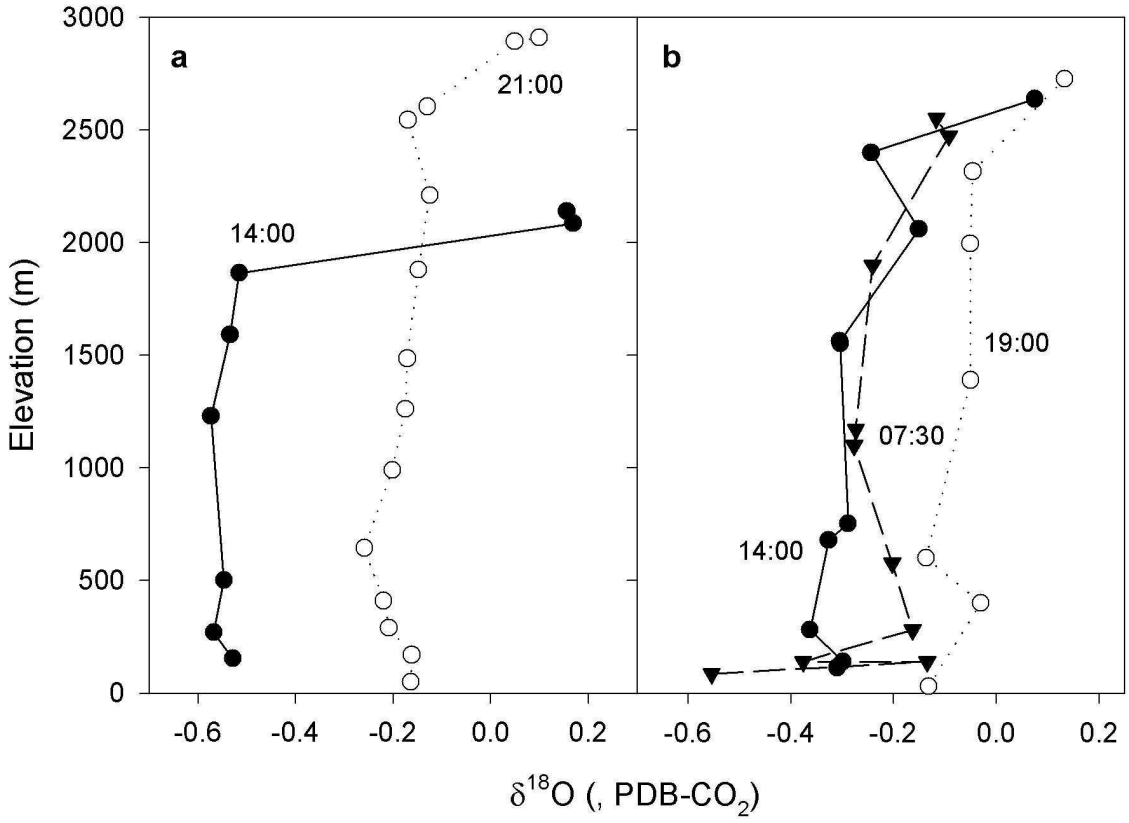

Figure 3.4: Profiles of $\delta^{18}O$ composition of CO_2 on (a) 23 July 1998 and (b) 24 July 1998. Symbols indicate where flask samples were taken. Solid line with filled circles is the afternoon profile (14:00 on each day), dotted line with open circles is the evening profile (21:00 on 23 July, 19:00 on 24 July) and dashed line with filled triangles is the morning profile (07:30 on 24 July).

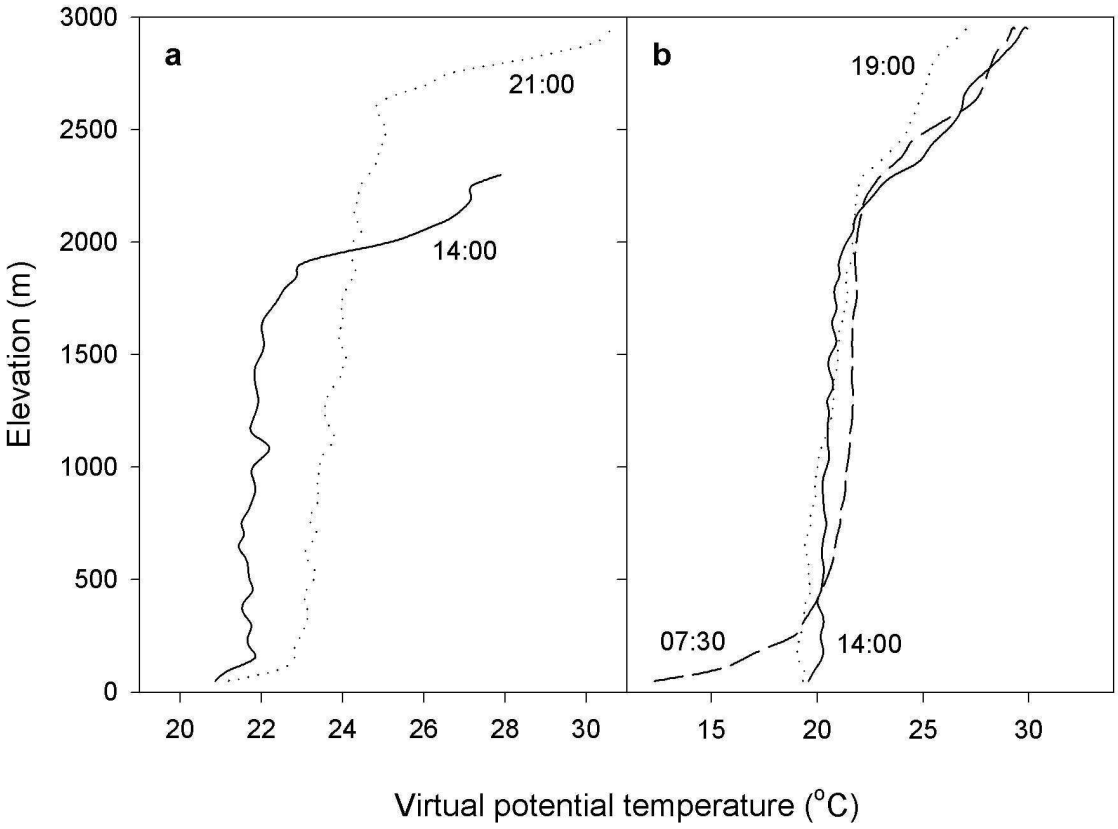

Figure 3.5: Profiles of virtual potential temperature on (a) 23 July 1998 and (b) 24 July 1998. Temperature was monitored continuously and averaged over each 50-metre interval. Solid line is the afternoon profile (14:00 on each day), dotted line is the evening profile (21:00 on 23 July, 19:00 on 24 July) and dashed line is the morning profile (07:30 on 24 July).

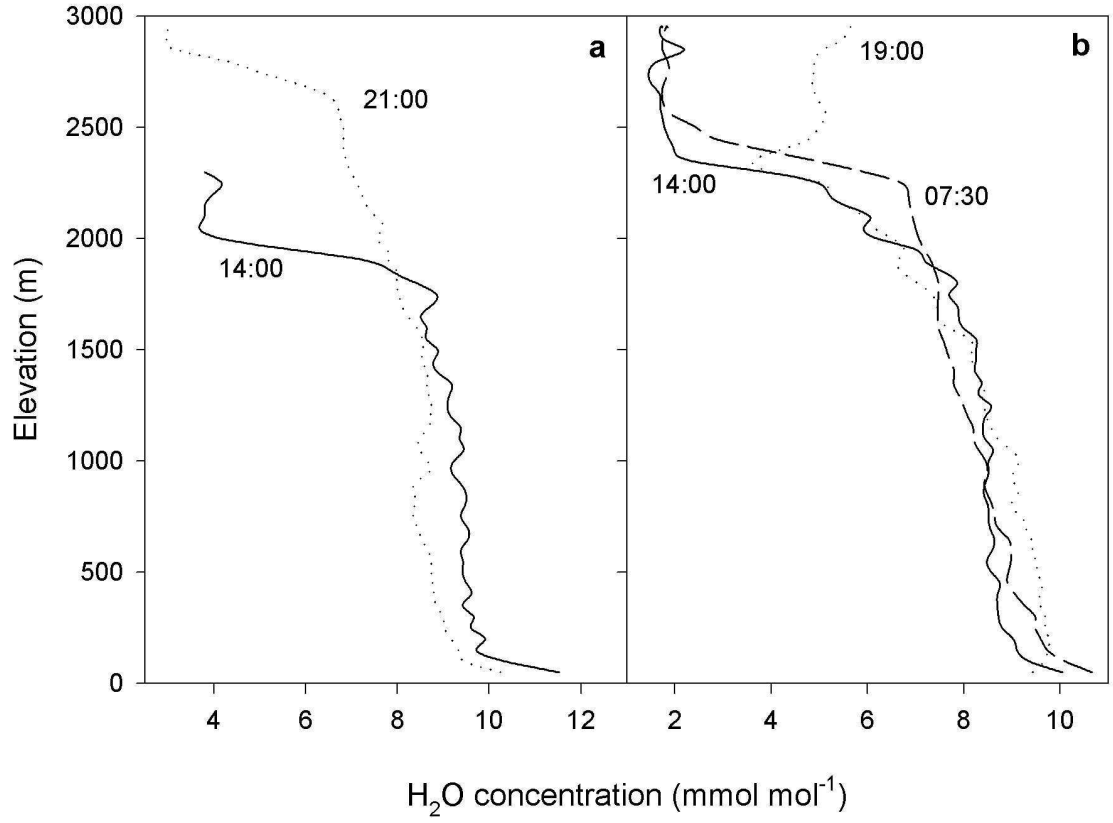

Figure 3.6: Profiles of H_2O concentration on (a) 23 July 1998 and (b) 24 July 1998. Concentration was monitored continuously and averaged over each 50-metre interval. Solid line is the afternoon profile (14:00 on each day), dotted line is the evening profile (21:00 on 23 July, 19:00 on 24 July) and dashed line is the morning profile (07:30 on 24 July).

between transpiration and assimilation. The dynamics of the NBL had little influence on H_2O concentrations.

The morning flight on 24 July indicated the presence of a residual layer representing the previous day's CBL. The data for this flight were treated in two different ways. Firstly, residual layer concentrations were used in place of mixed layer concentrations in Equation (3.2). The NBL was ignored, with its influence accounted for only by its effect on measured concentrations in the afternoon. The residual layer of the morning profile represented the state of the mixed layer the previous day when the vegetated surface became a net sink for sensible heat, thermal convection halted, and net ecosystem CO_2 exchange became positive (at around 2100 h according to the eddy covariance measurements of heat and CO_2 flux). The afternoon profile showed the change in mixed layer concentration due to development of the new CBL including mixing in of the NBL and entrainment of the residual layer, as well as the influences of surface exchange occurring in the period between the two flights and subsidence. Based on the sharp concentration gradient at around 100 m height, it was assumed that at the time of the morning flight NBL concentrations had not mixed into the residual layer at all. The flux calculated from the 0730 h and 1400 h flights on 24 July by the ICBL method in this case represented average surface flux overnight (locked up in the NBL) plus flux in the morning period between flights, with a total integrating time of 17 hours. Application of this approach to sensible heat was complicated by the term involving the square of the boundary layer height (or $M_B h$) in Equation (3.9). In this case it was necessary to account for the drop in boundary layer height overnight as it affected the vertical temperature gradient above the boundary layer. Hence an additional term was added to Equation (3.9) to allow for the overnight changes occurring above the boundary layer, obtaining:

$$\begin{aligned}\langle F_H \rangle &= \frac{(\Delta_{\theta 1} M_{B1} - \Delta_{\theta RL} M_{RL})}{T} + \langle \Delta_\theta \rangle \langle W_+ \rangle \\ &\quad + \frac{\frac{\gamma_\theta}{2}(M_{B1} h_1 - M_{RL} h_{RL})}{T_1} - \frac{\frac{\gamma_\theta}{2}(M_{RL} h_{RL} - M_{B0} h_0)}{T_0}\end{aligned}$$

where RL refers to the residual layer and this is treated here as extending to the ground; times t_0 and t_1 refer to the previous evening on 23 July and the afternoon on 24 July, respectively; the integrating periods T_0 and T_1 refer to the overnight and morning periods, respectively; and $T = T_0 + T_1$.

In the second treatment of the residual layer and NBL, surface flux for the morning period on 24 July (from 0730 h to 1400 h) was calculated by treating the NBL as the mixed layer. Here residual layer concentrations were used for air entrained during CBL growth, but entrainment due to the mean vertical velocity was assumed to carry tropospheric concentration. A possible source of error with this interpretation is that it is assumed that entrainment stops as soon as the entire residual layer has been incorporated. Residual layer entrainment usually occurs very quickly in the morning (Stull, 1988), so that further CBL growth would require entrainment of free tropospheric air. Neglect of this contribution would tend to underestimate surface CO_2 uptake, but since CBL growth is much slower once the residual layer has been assimilated and the stable free tropospheric air is reached, this contribution should be small. In the calculation of sensible heat fluxes by this approach it was necessary to account for the small but non-zero vertical gradient of $0.0015°\mathrm{Cm}^{-1}$ in virtual potential temperature within the residual layer, incorporated into the growing CBL.

Boundary layer heights and average CO_2 concentration, isotopic composition of CO_2, H_2O concentration and temperature within and above the CBL used in the budget methods are shown in Table 3.1. Regional respiration was assigned as that measured by eddy covariance at the forest site (Lloyd *et al.*, 2002b). Data were screened for low friction velocity and a respiration model was used for interpolation as described in Shibistova *et al.* (2002). Respiration rates for the four integration periods were thus found to be 2.85, 2.77, 2.37 and 2.52 μmol $\mathrm{m}^{-2}\mathrm{s}^{-1}$, respectively, for the periods PM 23 July, night+AM 23-24 July, AM 24 July and PM 24 July. Carbon isotopic composition of respired CO_2 was estimated as -26‰ (PDB-CO_2) from regression of night-time δ^{13}C versus inverse CO_2

concentration in the forest (Keeling, 1958; 1961, regression had equation $y = 6700x - 26$, $r^2 = 1.00$). Oxygen isotopic composition of respired CO_2 was estimated as -15‰ (PDB-CO_2) from rain water composition minus fractionation during equilibration with soil water (41.2‰ at 25°C, O'Neill *et al.*, 1975) and diffusion through the soil (-7.2‰ , Miller *et al.*, 1999). Oxygen isotope composition of recent rainwater was measured as -8‰ (SMOW). Regression of oxygen isotope composition with inverse CO_2 concentration using the few flask samples obtained within the NBL also suggested a respired CO_2 oxygen isotope composition of -15‰ .

Flight time	14:00 23 July	21:00 23 July	07:30 24 July	14:00 24 July	19:00 24 July
h (m)	1850	2650	2350	2300	2150
C_N (μmol mol^{-1})			377.8		
C_B (μmol mol^{-1})	350.7	352.1	353.3	353.0	351.5
C_+ (μmol mol^{-1})	358.6	357.9	359.4	359.7	358.4
$\delta^{13}C_N$ (‰)			-8.02		
$\delta^{13}C_B$ (‰)	-7.27	-7.36	-7.38	-7.37	-7.26
$\delta^{13}C_+$ (‰)	-7.72	-7.66	-7.72	-7.74	-7.62
$\delta^{18}O_N$ (‰)			-0.47		
$\delta^{18}O_B$ (‰)	-0.70	-0.18	-0.25	-0.31	-0.08
$\delta^{18}O_+$ (‰)	0.16	0.07	-0.11	-0.08	0.04
e_N (mmol mol^{-1})			10.38		
e_B (mmol mol^{-1})	9.26	8.24	8.11	8.17	8.55
e_+ (mmol mol^{-1})	3.90	2.93	1.84	1.76	4.82
θ_N (°C)			11.90		
θ_{N+} (°C)			18.83		
θ_B (°C)	21.85	23.74	20.76	20.68	20.26
θ_+ (°C)	26.97	28.08	27.09	26.58	24.71

Table 3.1: Boundary layer height (h), average CO_2 concentrations (C), carbon and oxygen isotopic composition of CO_2 ($\delta^{13}C$ and $\delta^{18}O$), H_2O concentration (e) and virtual potential temperature (θ) within (subscript B) and above (subscript $+$) the convective boundary layer measured for each flight. Values for the nocturnal boundary layer (subscript N, estimated height 100m) on the morning of 24 July 1998 are also shown, and the subscript B for this flight refers to the residual layer. The subscripts $+$ and $N+$ for temperature refer to just above the CBL and NBL, respectively.

3.3.3 Estimation of regional CO_2, latent heat and sensible heat fluxes and isotopic discrimination

The height integration method was applied using Equations (3.5) to (3.7) to show the effect of the density and subsidence corrections to the method, with 50-metre height intervals up to 3000 metres (referred to as "height integration, $\Delta z = 50$"). The method was also applied using Equation (3.7) with only two integration layers representing within and above CBL concentrations for the two sampling times (referred to as "height integration, two-layer"). For the morning profile on 24 July three layers were required, representing the NBL, residual layer and free troposphere. An estimate of overnight and morning flux could also be obtained by this method in the same manner as for the ICBL method, by extending the residual layer and its average concentration to the ground as it would have been the previous evening.

CO_2 flux and isotopic discrimination were calculated for the afternoon of 23 July, overnight and morning of 23-24 July, morning of 24 July and afternoon of 24 July using both the integral CBL budget equation and the height integration method (Tables 3.2 and 3.3). Also shown in Table 3.2 are comparisons of the height integration method with and without correction for air loss due to column expansion (ρ correction) and for subsidence (w_+ correction). Reasonable agreement was found between flux and discrimination estimates by the two methods when ρ and w_+ corrections were applied, though the CO_2 flux estimates differ by 40% for the afternoon period of 24 July. Eddy covariance measurements of CO_2 flux from the forest and bog towers were averaged over each integrating period for comparison with the CBL budget estimates. Table 3.2 shows that CO_2 flux estimates by the ICBL method agree well with the eddy covariance measurements in the forest.

The ICBL budget method was used to estimate sensible and latent heat fluxes for the same periods. Table 3.4 shows that latent heat flux obtained by the budget method was closer to that measured in the bog for the first two averaging periods, and to the forest measurements for the remaining periods. While no significant difference was observed between water vapour profiles obtained over the forest and bog for any flight, the high

CO_2 flux (μmol $m^{-2}s^{-1}$)	PM 23 July	Night+AM 23-24 July	AM 24 July	PM 24 July
ICBL budget equation (Equation (3.4))	-4.1	-1.9	-7.2	-6.6
ICBL budget equation using flask data (Equation (3.4))	-3.9	-2.1	-6.1	-7.3
Height integration: Δz=50m (Equation (3.5))	-5.8		-3.6	-13.5
Height integration: Δz=50m with ρ correction (Equation (3.6))	-2.8		-3.4	-7.6
Height integration: Δz=50m with ρ and w_+ correction (Equation (3.7))	-4.7		-5.1	-9.4
Height integration: 2-layer with ρ and w_+ correction (Equation (3.7))	-4.8	-1.8	-6.1	-8.5
Eddy covariance: forest tower	-4.1	-1.8	-6.9	-7.0
Eddy covariance: bog tower	-2.6	-1.7	-3.6	-4.2

Table 3.2: CO_2 flux calculated from the integral CBL budget and height integration methods, and measured by eddy covariance. Except for the second row, results are obtained using IRGA CO_2 data.

latent heat flux estimated for the afternoon on 23 July may indicate that the air mass sampled for those flights was influenced by bog exchange (as shown also in the methane and ^{18}O profiles). Sensible heat fluxes showed a similar pattern with respect to eddy covariance measurements, with estimates for the afternoon on 23 July and overnight plus morning 23-24 July being lower than estimates for the morning and afternoon of 24 July. Agreement between ICBL budget regional flux estimates and eddy covariance measurements was generally good for both latent heat and sensible heat.

Budget estimates for CO_2, latent heat and sensible heat are superimposed on the measured diurnal variation in fluxes at the forest and bog sites in Figure 3.7. It is clear from this figure that the CBL budget estimates were generally close to the eddy covariance measurements in the forest.

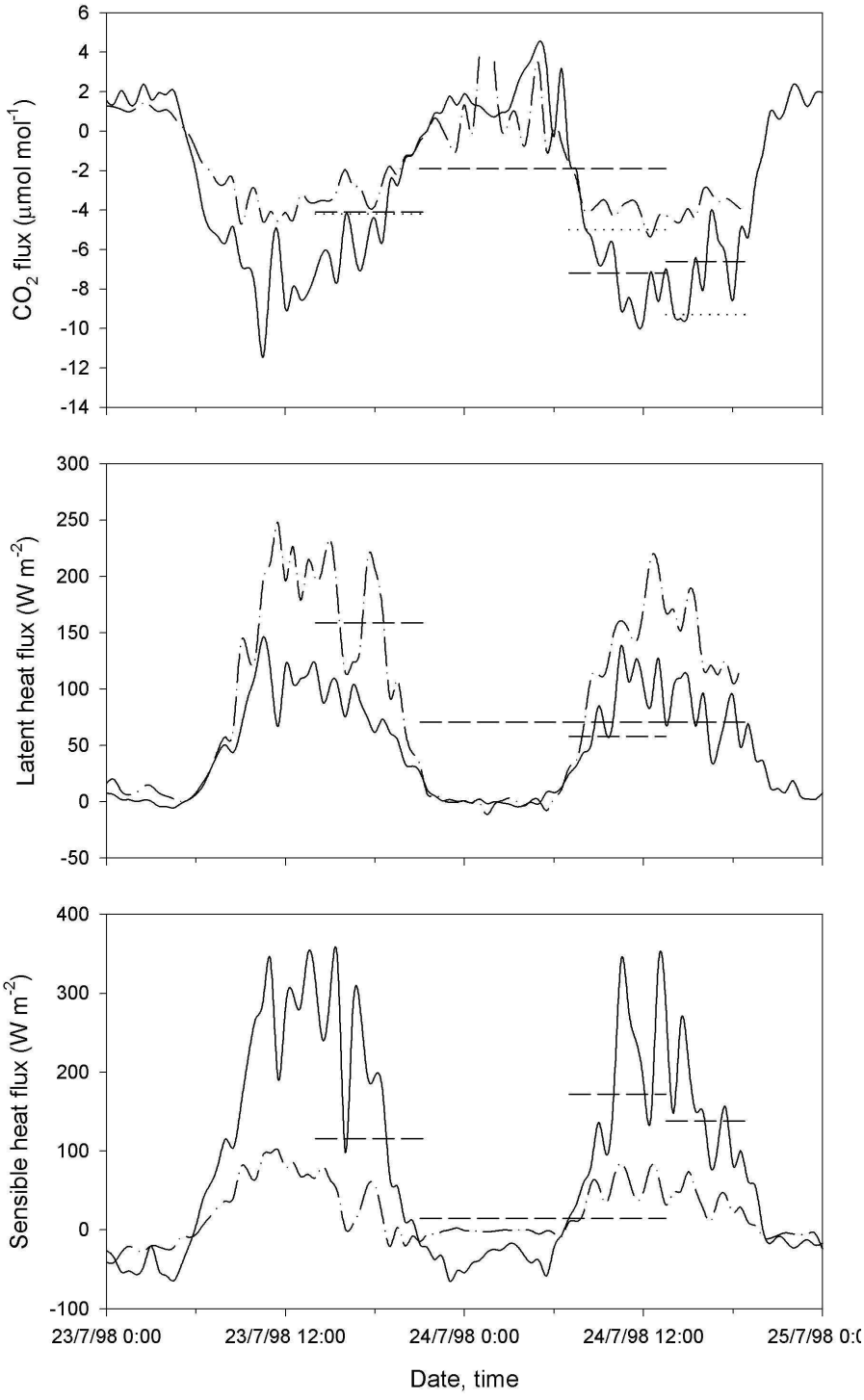

Figure 3.7: Measured and modelled CO_2, latent heat and sensible heat fluxes, 23-24 July 1998. Solid lines are the eddy covariance flux measurements over the forest; dash-dot lines those over the bog; dashed lines are the ICBL budget method estimates; and dotted lines are the multilayer height integration method estimates for CO_2 flux only, with density and subsidence correction.

Δ_A (‰)	PM 23 July	Night+AM 23-24 July	AM 24 July	PM 24 July
ICBL budget equation Δ^{13}C (Equation (3.4))	19.0	18.1	17.2	21.8
Height integration: 2-layer with ρ and w_+ correction Δ^{13}C (Equation (3.7))	19.9	18.0	17.7	22.9
ICBL budget equation Δ^{18}O (Equation (3.4))	37	-1	-5	43
Height integration: 2-layer with ρ and w_+ correction Δ^{18}O (Equation (3.7))	48	0	-4	40

Table 3.3: Carbon and oxygen isotope discrimination calculated from the integral CBL budget and height integration methods. The CO_2 flux estimates required for the calculations were those obtained from the flask data using the same method as for the isotope calculations.

Latent (LE) and sensible (H) heat flux (W m^{-2})	PM 23 July	Night+AM 23-24 July	AM 24 July	PM 24 July
ICBL budget equation LE (Equation (3.4))	159	71	58	71
Eddy covariance: forest tower LE	66	35	85	78
Eddy covariance: bog tower LE	141	62	156	133
ICBL budget equation H (Equation (3.4))	116	15	172	138
Eddy covariance: forest tower H	147	53	184	138
Eddy covariance: bog tower H	19	21	56	37

Table 3.4: Latent (LE) and sensible (H) heat flux calculated from the integral CBL budget and measured by eddy covariance.

3.4 Discussion

3.4.1 Carbon dioxide fluxes

The CBL budget methods are very sensitive to measurement errors, since the flux that is sought is often the small difference between large terms. In particular, a significant subsidence term can change the sign of the inferred flux. Despite this, the flux estimates obtained by the ICBL budget method agreed very well with eddy covariance measurements made over the forest site (within 10%). Eddy covariance measurements over the bog site were considerably lower (Table 3.2, Figure 3.7). No significant difference was found between CBL concentration profiles taken over forest and bog regions with one exception, indicating that the turbulent mixing in the CBL had likely smoothed the two influences. The exception was the afternoon profile of $\delta^{18}O$ on 23rd July, in which oxygen isotope composition for the bog profile was depleted by around 0.2‰ (not shown). Methane concentrations were also higher for this profile (not shown). These data were not used in the analysis, and it seems likely that except for this case the profiles were dominantly influenced by forest exchange processes. In general under typical weather conditions, flux estimates from ICBL methods have source footprints of about 1000 km^2 (Cleugh and Grimmond, 2001). This is in the order of the scale of heterogeneity of the landscape of this study, so it was somewhat surprising that the observations implied mixing was occurring over a larger scale.

CO_2 flux estimates obtained by the height integration method were reasonably close to eddy covariance measurements in the forest (within 35%) when the corrections for air loss and subsidence were applied. Without these corrections values were unsystematically and considerably different from measurements (Table 3.2). The estimates obtained using only two layers in the integration (within and above the CBL) were similar to those obtained with the full integration (Table 3.2). This allowed the height integration method to be used for isotopes, where continuous data were unavailable. To investigate the effect of having only few concentration data at discrete heights as in the isotopic calculations, flux

estimates for CO_2 were calculated by the ICBL method using only concentrations obtained from flask analysis (Table 3.2). Values thus found were also in reasonable agreement with the forest surface measurements, suggesting that little error could be attributed to vertical heterogeneity in CBL or tropospheric concentrations.

As mentioned earlier, the subsidence term increased the magnitude of inferred CO_2 uptake by about 1.8 μmol $m^{-2}s^{-1}$, which may be taken as an upper limit on the error introduced by the estimate of w_+. Flux estimates obtained using the NCEP model estimates for w_+ give results close to the bog tower measurement on the first afternoon, but closer to the tower measurements in the morning and afternoon of the second day. This could be interpreted as consistent with the observations of ^{18}O composition and methane concentrations indicating a larger bog influence in the afternoon of 23 July. Notably, flux for the overnight and morning period is significantly underestimated with lower w_+. This lends support to the validity of the value of -0.008 ms^{-1} estimated from the overnight drop in boundary layer height. It should be noted, however, that eddy covariance measurements are most subject to error at low wind speeds which typically occur overnight, and may underestimate night time respiration if mass is lost through advection. For the study here the friction velocity was relatively high overnight (greater than 0.3 ms^{-1}) and little error was expected from this effect (see Shibistova *et al.*, 2002). Extrapolation of the estimated subsidence velocity to the previous and next day may be justified to some extent by the presence of a large, slow-moving high pressure cell over the region at the time, limiting the pace of changes in synoptic conditions (Figure 3.1).

3.4.2 Isotopic discrimination

Carbon isotopes

Values obtained for $\Delta^{13}C$ ranged from 17‰ to 22‰ , with the two budget methods agreeing well. These values correspond to a range of c_i/c_a from 0.6 to 0.8 (Table 3.3), and are comparable with other estimates for this biome in the literature. Global model estimates for boreal coniferous forests range from 15-16‰ (Lloyd and Farquhar, 1994; Bakwin *et al.*, 1998) to 20‰ (Fung *et al.*, 1997, with seasonal amplitude ∼1‰). Field measurements in

a boreal pine forest found $\Delta^{13}C = 19‰$ (Flanagan *et al.*, 1996). Leaf $\delta^{13}C$ was measured as -27 to -28‰ (PDB-CO_2), which with a mean CBL value of ∼-7‰ (PDB-CO_2) implies an average $\Delta^{13}C$ of 20 to 21‰. It should be noted that these other estimates are all representative of the annual mean, while the study here represents only two days in the middle of the growing season.

Diurnal variation in $\Delta^{13}C$ would normally be expected to behave in a sense opposite to that observed, since stomatal conductance and c_i would be relatively high in the morning when vapour pressure deficit is low, leading to higher carbon isotope discrimination. The value estimated here for the morning of 24 July of 17‰ is lower than expected, and is perhaps affected by errors in the application of the CBL model, particularly in the incorporation of the residual boundary layer to the model and/or advective losses. The sparse sampling of CBL concentrations provided by flask collection may also limit the accuracy of flux estimates. Comparison of CO_2 flux estimates using flask and IRGA data for the morning period of 24 July (corresponding to the low $\Delta^{13}C$ estimate) shows that for this period the estimate from flask data was in much poorer agreement with forest eddy covariance measurements than that from IRGA data (Table 3.2). Agreement between flux estimates from flask and IRGA data for other periods was much better.

Oxygen isotopes

The estimates obtained for $\Delta^{18}O$ varied from around 40‰ for the afternoon periods to -5‰ for the morning period. Estimates from the two budget methods agreed reasonably well. With c_i/c_a calculated from $\Delta^{13}C$, c_c approximated by c_i and $\Delta^{18}O$ obtained from the CBL budget, the fractionation model described in §3.1.4 can be used to determine δ_c and hence δ_S (Table 3.5). Due to the sandy soil in the pine forest area with low water-holding capacity, isotopic composition of source water should be close to that of recent precipitation, so the calculated value for δ_S could be used to validate the modelled oxygen isotope discrimination. Atmospheric vapour was assumed to be in isotopic equilibrium

with source water and e_a/e_i was equated to relative humidity as measured at the eddy covariance tower in the forest. The estimates obtained for Δ^{18}O by the two budget methods agreed reasonably well for all periods (Table 3.3).

	PM 23 July	Night+AM 23-24 July	AM 24 July	PM 24 July
Δ^{13}C (‰)	19.0	18.1	17.2	21.8
Δ^{18}O (‰)	37	-1	-5	43
c_i/c_a	0.65	0.61	0.57	0.77
e_a/e_i	0.36	0.52	0.47	0.43
δ_c (‰)	15	-6	-10	10
δ_S (‰)	-7	-23	-28	-10

Table 3.5: Ratio of intercellular to ambient CO_2 concentration (c_i/c_a) calculated from carbon isotope discrimination (Δ^{13}C); and isotopic composition of chloroplast (δ_c) and source (δ_S) water calculated from oxygen isotope discrimination (Δ^{18}O) and ratio of ambient to intercellular vapour pressure (e_a/e_i). Isotope discriminations are those found using the integral CBL budget method with flask CO_2 data.

The last significant rainfall before the flights was three weeks earlier, and its isotopic composition was measured as -8‰ (SMOW). Composition of earlier rainfall ranged from -6‰ to -18‰ (SMOW). Soil evaporation between rain events would tend to enrich soil water composition. This would suggest that the estimates for source water of -7‰ and -10‰ (SMOW) for the afternoon periods of 23 and 24 July respectively were reasonable, whereas the values obtained for the intervening periods are overly depleted (Table 3.5).

Concentration of CO_2 at the sites of carboxylation is likely to be lower than in the intercellular spaces (Evans and von Caemmerer, 1996); however a lower c_c results in an even more negative estimate of δ_S for the night and morning periods. Similarly, a lower value of e_a/e_i should be used when weighted by assimilation rate but this also reduces the estimated source water composition. Isotopic composition of chloroplast water is likely to be less enriched than the Craig-Gordon (CG) model predicts. Observations for bulk leaf water are indeed less enriched (Flanagan, 1993; Wang *et al.*, 1998), and can be explained alternatively by the presence of several mixing pools (Yakir *et al.*, 1989) or by opposing diffusion and convection from the sites of evaporation (the Péclet effect, Farquhar and

Lloyd, 1993; see also review by Yakir, 1998 for discussion of various leaf water isotopic models). Wang *et al.* (1998) found that divergence of composition of chloroplast water from that predicted by the CG model increased with increasing Péclet number, but in contrast to other species, the single species of conifer they measured was well described by the CG model. Nevertheless, a more positive value for composition of water at the sites of evaporation than the approximation given by chloroplast water, as found in most cases, implies a more positive value for source water, which may help to reconcile the results found here.

The Craig-Gordon model used here to estimate isotopic composition of water at the sites of evaporation applies to steady-state conditions only. Overnight it would be expected that chloroplast water would eventually equilibrate with source water and it would take some time in the morning as the stomata open for the isotopic composition to move toward the steady-state Craig-Gordon value. Observations and model estimates by Cernusak *et al.* (2002) in Lupin suggest that, depending on the imbalance between transpiration and xylem flow, this effect can maintain leaf water compositions of up to 5‰ below steady state values. This disequilibrium could therefore be sufficient to maintain the depleted Siberian source water signature in the chloroplasts and produce the negative discrimination that was modelled for the morning period.

Another important process that may help to explain the apparent very negative source water composition is possible covariance of c_i/c_a and chloroplast CO_2 isotopic composition (δ_c) between the forest and bog sites. Table 3.6 shows a simple calculation assuming much higher c_i and more negative δ_c in the bog compared to the forest. The oxygen isotope discrimination $\Delta^{18}O$ calculated for the aggregated bog and forest areas assuming an area ratio of 1:4 using these values is the same as was found by the integral CBL budget calculation for the morning of 24 July (Table 3.3). It can be seen from Table 3.6 that the source water composition calculated from the aggregated discrimination is much more negative than that calculated for each of the bog and forest areas separately, using their individual values for δ_c and e_a/e_i. Calculation of aggregated carbon isotope discrimination

Δ^{13}C with the assigned values for c_i/c_a in this example is also consistent with the value found by the ICBL budget method for AM 24 July (Table 3.3), but values for the bog and forest differ considerably. The example in Table 3.6 is exaggerated to illustrate the idea and discrimination was not weighted according to the relative assimilation rates of the bog and forest areas, but assigned values are not beyond the realms of possibility. The inferred bog source water composition is still more negative than measured values in the bog (-14‰ , SMOW) and surrounding creeks (-18‰ , SMOW), but is much closer than the estimate of -28‰ obtained from the aggregated data.

Area	c_i/c_a (assigned)	e_a/e_i (measured)	δ_c (assigned)	δ_s (calculated)	Δ^{18}O (calculated)	Δ^{13}C (calculated)
Bog	0.90	0.63	-10.00	-22.95	-73.00	24.74
Forest	0.48	0.46	4.00	-14.90	12.62	15.25
Forest+bog	0.56[1]	0.49[1]	-10.67[2]	-28.38[2]	-4.51[1]	17.15[1]

[1]Calculated as 0.2×bog + 0.8×forest; [2]Calculated from aggregated Δ^{18}O value.

Table 3.6: Example calculation of the effect of aggregation of bog and forest areas when c_i/c_a and δ_c covary.

In other studies, diurnal variation in Δ^{18}O has been modelled from leaf water measurements to range from around -5‰ during the night and morning to +20‰ in the afternoon for a boreal pine forest with precipitation of similar isotopic composition (Flanagan *et al.*, 1997), though humidity may not have been comparable to the present case. A global oxygen isotope discrimination model estimated Δ^{18}O ∼8‰ for the Zotino area based on a precipitation estimate of -18‰ (SMOW, Farquhar *et al.*, 1993). The larger values found for the afternoon periods in this study (40-50‰) may indicate that the low humidity in the afternoons at the study site (∼40%) is producing greater evaporative enrichment of leaf water than was present or estimated in the studies mentioned above.

3.4.3 Sensible and latent heat fluxes

In addition to the sources of error already discussed in relation to CO_2 flux estimates, a significant limitation to the accuracy of sensible heat flux predictions is the estimation of the vertical gradient in virtual potential temperature γ_θ above the boundary layer. The

term involving γ_θ is as significant as the subsidence term in the sensible heat budget. It is very sensitive to the value of γ_θ: an increase in this parameter of 10% led to increases in the inferred sensible heat flux of up to 20% in this study. While the gradient can be measured, the profiles in Figure 3.5 show that substantial natural variations exist, which cannot be quantified in the simplified budget used here.

Neglect of the γ term (that is, the assumption that $\gamma = 0$) may also be a source of error for both the CO_2 and H_2O budgets if there exists any concentration gradient above the boundary layer. The measured concentration profiles showed no such gradient, but for example including a very small gradient in water vapour concentration of -0.0005 mb m^{-1} changed the inferred latent heat fluxes by up to 50%, in either direction depending on whether the boundary layer height had increased or decreased during the integration period.

With best estimates for the parameters entering the budget equations, however, the inferred regional fluxes for sensible and latent heat by the ICBL method were generally reasonably close to the flux magnitudes to be expected for the region, as indicated by the eddy covariance measurements. The height integration method was not applied to sensible and latent heat because the measurements were of poorer quality than for CO_2 and errors due to variations at the top of the integrating column were greater.

3.4.4 Budget method comparison

The height integration method undertakes a straightforward mass difference approach, which relies only on the assumption of no advection and temporally constant concentration at the top of the integrating column. The ICBL budget method also assumes no advection, in addition to constant concentration within the mixed layer (the CBL) and in the free troposphere (above the CBL). While the ICBL budget method assumptions will not be strictly true, they may be beneficial in smoothing noisy measurement data. Concentrations of layers contributing to the height integration method are susceptible to the natural heterogeneity of the atmosphere and may be skewed by an unrepresentative air mass,

particularly near the ground where they are in closer proximity to the source of variation (surface heterogeneity) and are weighted by higher density. Averaging samples within and above the CBL as in the ICBL budget method significantly reduces this potential for bias.

The necessity of including subsidence and correcting for change in total air mass in the height integration method also demonstrates weakness in the method. These corrections bring the method closer to the ICBL budget approach, where knowledge of boundary layer development is utilised to interpret changes in concentration over the day.

It was noted earlier that the height integration equation (Equation (3.5)) reduced to the ICBL budget equation (Equation (3.2), without the subsidence term) when the two layers corresponding to within and above CBL were chosen. In practice, however, there are factors complicating this equality such as vertical contraction or expansion of the integrating column (the density correction), as well as variation of free tropospheric CO_2 concentration with time, which is not accounted for in the height integration method. If average free tropospheric concentrations are used between the two profiles over the integration period, then the two-layer height integration method (Equation (3.7), including density and subsidence corrections) agrees identically with the ICBL method (Equation (3.4)) except for the morning period on 24 July, where the treatment of the residual layer causes a difference of 0.3 μmol $m^{-2}s^{-1}$ between the methods (see discussion below, p.117). This suggests that the main deficiency in the height integration method is the assumption of time-invariant CO_2 concentrations at the top of the integrating column, and that this deficiency can perhaps be overcome by estimation of the rate of this change and appropriate correction. The correction may readily be applied by use of averages in the two-layer case, but could be incorporated as an additional term in the multilayer case in a manner analogous to the density correction, utilising observed differences in free tropospheric concentrations between the profiles. The data presented here suggest that the additional resolution of the multilayer height integration (more appropriate weighting of concentrations according to density at each level) does not significantly improve flux estimates, perhaps

because the variation in concentrations with height within and, separately, above the CBL was reasonably small (see Figure 3.2).

The importance of the treatment of variation of free tropospheric concentrations in time is also evident in the ICBL budget method. Very different results are obtained when Equation (3.2) is used with the difference between above- and within-CBL concentrations for each profile independently ($c_{Bi} - c_{+i}$ at time t_i, with values given in Table 3.1). The implicit assumption in Equation (3.2) is that free tropospheric concentrations are constant in time. This gives flux estimates of -1.6, -2.4, -7.2 and -0.5 μmol m^{-2}s^{-1} for the periods corresponding to PM 23 July, night+AM 23-24 July, AM 24 July and PM 24 July, respectively, in much poorer agreement with the eddy covariance measurements than when average free troposphere concentrations are used (Equation (3.4)). The morning period of 24 July is not affected because the residual layer rather than the free troposphere is entrained during CBL growth.

The difference between the ICBL budget method and the two-layer height integration method when time-averaged tropospheric concentrations were used in the latter method for the morning of 24 July can be determined from Equations (3.4) and (3.7) as:

$$(F_{c,2HI} - F_{c,ICBL})_{AM\ 24\ July} = \frac{(c_{RL} - \langle c_+ \rangle)\,(M_{B1} - M_{B0})}{T}$$

where $2HI$ refers to the two-layer height integration method; the subscript RL refers to the residual layer; and $M_{B0} = M_N + M_{RL}$, the sum of moles of air in the NBL and residual layer. This can be interpreted as accounting for the additional growth of the CBL beyond the height of the residual layer, where tropospheric concentrations are entrained. Recall that the treatment of the NBL and residual layer in the ICBL method for the morning of 24 July assumed no such additional entrainment. In this case, the height of the boundary layer in the afternoon was actually less than that of the residual layer in the morning by 50 metres (Table 3.1). The principle applies equally well here because the whole of the residual layer would have been entrained into the growing boundary layer, rather than all but the last 50 metres. Hence the height integration method has shown that it is

important to take account of the evolution of the boundary layer beyond the point at which the residual layer is fully entrained. The ICBL budget may easily be rectified to include this contribution by adding the term shown in the equation above.